RSC Advances

PAPER

View Article Online
View Journal | View Issue

Cite this: *RSC Adv.*, 2018, **8**, 37550

Optimized $NiCo_2O_4$/rGO hybrid nanostructures on carbon fiber as an electrode for asymmetric supercapacitors

Hui Jiang,[a] Kang Yang,[a] Pingwei Ye,[b] Qiang Huang,[b] Lingyun Wang[b] and Sumin Li *[a]

Received 7th September 2018
Accepted 22nd October 2018

DOI: 10.1039/c8ra07477a

rsc.li/rsc-advances

The $NiCo_2O_4$ nanowires and reduced graphene oxide (rGO) hybrid nanostructure has been constructed on carbon fibers ($NiCo_2O_4$/rGO/CF) *via* a hydrothermal method. The effects of graphene oxide (GO) concentration on the structure and performance of the $NiCo_2O_4$/rGO/CF were investigated in detail to obtain the optimized electrode. When the GO concentration was 0.4 mg ml^{-1}, the rGO/$NiCo_2O_4$/CF composite exhibited a maximum specific capacitance of 931.7 F g^{-1} at 1 A g^{-1}, while that of $NiCo_2O_4$/CF was 704.9 F g^{-1}. Furthermore, the $NiCo_2O_4$/rGO/CF//AC asymmetric supercapacitor with a maximum specific capacitance of 61.2 F g^{-1} at 1 A g^{-1} was fabricated, which delivered a maximum energy density (24.6 W h kg^{-1}) and a maximum power density (8477.7 W kg^{-1}). Results suggested that the $NiCo_2O_4$/rGO/CF composite would be a desirable electrode for flexible supercapacitors.

1. Introduction

Recently, much attention has been paid to developing flexible supercapacitors due to their potential applications in wearable electronic devices.[1–4] Conductive carbon fibers, metal foils and foams have served as platforms for depositing nanostructured active materials to construct flexible supercapacitor electrodes. In particular, continuous three-dimensional carbon materials including carbon fiber fabrics, textiles and cloths have received increasing attention owing to their advantages, such as high corrosion resistance, outstanding electrical conductivity, low cost and porous structure. To achieve high-performance flexible supercapacitors, they have been widely used as frameworks to construct hybrid nanostructures.[5–10] Especially, some metal oxides (*e.g.*, Co_3O_4, MnO_2, $NiCo_2O_4$, Fe_2O_3, NiO, $CoMoO_4$, *etc.*) decorated on carbon textiles as flexible electrodes for supercapacitors have been developed.[5,11–20] Among various metal oxide electrode materials, $NiCo_2O_4$ has been widely researched owing to its high theoretical capacity.[21,22] However, the electrochemical performance of $NiCo_2O_4$-based flexible electrode is restricted because of low electrical conductivity of $NiCo_2O_4$. Recent reports have confirmed that the introduction of conductive materials, for example PPy, could enhance the electrochemical performance of $NiCo_2O_4$-based flexible electrodes.[23,24]

Herein, in view of the good electrical conductivity of graphene, we have successfully constructed $NiCo_2O_4$ nanowires and reduced graphene oxide hybrid nanostructures on carbon fiber framework to obtain the novel $NiCo_2O_4$/rGO/CF composites, in which graphene sheets were decorated on the $NiCo_2O_4$ nanowires, forming the hierarchical structure. The as-obtained materials were used as supercapacitor electrodes and their electrochemical performance was investigated. The influences of GO on the composition, structure and electrochemical performance of $NiCo_2O_4$/rGO/CF electrodes were investigated in detail to obtain the optimized electrode materials.

2. Experimental

2.1. Synthesis of $NiCo_2O_4$/rGO hybrid nanostructures on CF ($NiCo_2O_4$/rGO/CF)

At first, $NiCo_2O_4$ nanowires were prepared *via* a hydrothermal method. 4 mmol $Co(NO_3)_2 \cdot 6H_2O$, 2 mmol $Ni(NO_3)_2 \cdot 6H_2O$ and 24 mmol urea were poured into 50 ml water–ethanol mixed solution (volume ratio 1 : 1) and sonicated to form homogeneous solution. Next, the mixture was added into a 100 ml autoclave, and a slice of CF cloth (2 × 5 cm^2) was put in. Then, the sample was heated to 120 °C and kept 8 h. At last, the as-prepared sample was washed with distilled water, and the NiCo-based precursor grown on CF cloth was obtained.

Urea was added to 50 ml 0.2–1.0 mg ml^{-1} GO (the mass ratio of urea to GO was 15 : 1) aqueous dispersion and sonicated for 6 h. Then, the mixture was poured into the autoclave, and the CF loaded with NiCo-based precursor was immersed into the solution. Next, the autoclave was kept at 120 °C for 8 h. After that, the as-obtained samples were dried at 60 °C for 12 h, followed by calcination at 350 °C for 2 h to obtain $NiCo_2O_4$/rGO hybrid nanostructures on CF cloth.

For comparison, a piece of $NiCo_2O_4$ nanowires on CF ($NiCo_2O_4$/CF) was prepared using the same procedure as $NiCo_2O_4$/rGO/CF.

[a]*School of Materials Science and Engineering, Jiangsu University, Zhenjiang 212013, China. E-mail: li_sm@ujs.edu.cn*

[b]*Research Institute of Chemical Defense, Beijing 100191, China*

2.2. Characterization

The microstructure of samples was characterized *via* a scanning electron microscopy (SEM, JEOL JSM-7001F) and a transmission electron microscopy (TEM, JEOL JEM-2010F). The crystal structure was analyzed *via* a X-ray diffraction (XRD, Bruker D8 ADVANCE).

The electrochemical characterizations, containing cyclic voltammetry (CV), galvanostatic charge/discharge (GCD) tests and electrochemical impedance spectroscopy (EIS), were conducted with a CHI660D electrochemical workstation. A three-electrode and two-electrode system were used to evaluate the electrochemical performance of the single electrodes and asymmetric supercapacitor (ACS) cell, respectively.

3. Results and discussion

3.1. Characterization of composition and microstructure

Fig. 1 shows the XRD patterns of $NiCo_2O_4$/rGO hybrids scratched down from CF with different concentrations of GO. It can be seen that there were similar diffraction peaks for all samples. Characteristic diffraction peak corresponding to graphene sheets ($2\theta \approx 25.1°$) had not been observed,[25,26] which may be due to its low diffraction intensity or highly disorderly structure.[27] The dominant peaks at 2θ values of 19.0°, 31.4°, 36.9°,44.9°, 59.6° and 65.5° were ascribed to the (111), (220), (311), (400), (511) and (440) planes of $NiCo_2O_4$ (JCPDS 01-073-1702), which confirmed the formation of $NiCo_2O_4$. According to the patterns, it could be concluded that the concentration of GO had no obvious influence on the crystal structure of $NiCo_2O_4$ nanowires.

The SEM images of carbon fiber and $NiCo_2O_4$/rGO/CF composites are shown in Fig. 2. It can be observed that much surface defects were observed on the surface of fiber (Fig. 2a), which is helpful for the growth of $NiCo_2O_4$ nanowires. From Fig. 2b–d, it is observed that the $NiCo_2O_4$ nanowires were uniformly and densely grown over the surface of carbon fibers. Among $NiCo_2O_4$ nanowires, graphene sheets or aggregates were observed, the smaller rGO sheets were embedded in the $NiCo_2O_4$ nanowires, while the larger rGO sheets were supported by the top of $NiCo_2O_4$ nanowires, forming the hierarchical structure. Especially, when the concentration of GO was 0.4 mg ml^{-1}, no rGO aggregates were observed, rGO and $NiCo_2O_4$ nanowires distributed uniformly on the surface of CF, forming the hierarchical porous nanostructure, in which rGO would act as good conductive pathway for fast electron transfer, which would be helpful for improving the electrochemical properties of electrode materials. However, with increasing GO concentration, graphene sheets aggregated and thus the $NiCo_2O_4$ nanowires were damaged (Fig. 2e and f). Especially when the concentration of GO was 1.0 mg ml^{-1}, $NiCo_2O_4$ nanowires collapsed seriously (Fig. 2f), resulting in the destruction of the hierarchical porous nanostructure. Subsequently, the migration of ions would be hindered due to massive graphene aggregation, and the electrochemical properties of electrode material would be influenced.

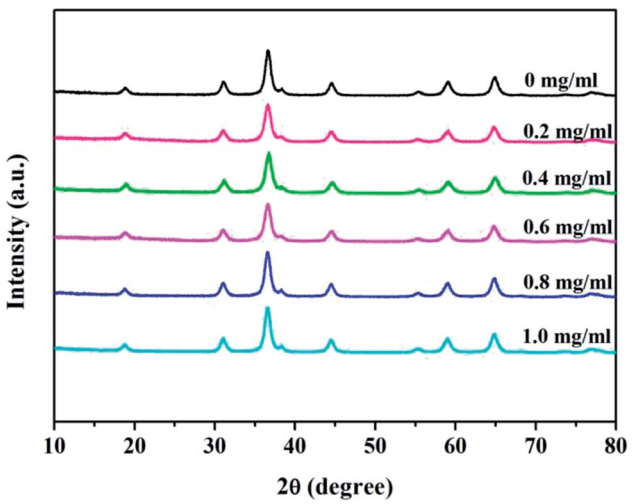

Fig. 1 XRD patterns of $NiCo_2O_4$/rGO with different GO concentrations.

The TEM and HRTEM images of individual $NiCo_2O_4$ nanowire are shown in Fig. 3. It can be seen that the average diameter of $NiCo_2O_4$ nanowire was approximately 40 nm (Fig. 3a). Moreover, as seen in the high-magnification TEM image (Fig. 3b), the $NiCo_2O_4$ nanowires were composed of nanocrystallites with the size of 5–10 nm, which was consistent with XRD results. Among nanocrystallites lots of nanopores were observed, forming highly porous structure.

3.2. Electrochemical performance of $NiCo_2O_4$/rGO/CF composites

The electrochemical performance of the as-obtained $NiCo_2O_4$/rGO/CF composites were investigated *via* a three-electrode system with the electrolyte of 3 M KOH solution, in which the $NiCo_2O_4$/rGO/CF, Ag/AgCl and Pt acted as the working electrode, reference electrode and counter electrode, respectively. Fig. 4a shows the CV curves of $NiCo_2O_4$/rGO/CF electrodes with different GO concentrations at 20 mv s^{-1} under the potential window of −0.2 to 0.6 V. It shows that a couple of redox peaks were obviously displayed for all the $NiCo_2O_4$/rGO/CF electrodes, suggesting the faradaic behaviors.[28] The redox mechanism of $NiCo_2O_4$ in KOH, and the possible faradaic reactions are represented as follows:

$$NiCo_2O_4 + OH^- + H_2O \leftrightarrow NiOOH + 2CoOOH + e^- \quad (1)$$

$$CoOOH + OH^- \leftrightarrow CoO_2 + H_2O + e^- \quad (2)$$

Fig. 4b presents GCD curves of $NiCo_2O_4$/rGO/CF electrodes at 1.0 A g^{-1} at potential window ranging from 0 to 0.42 V. Evidently, the GCD curves displayed nonlinear and poor symmetrical shapes, indicating the combination of electric double layer and pseudo-capacitance characteristic. According to the GCD curves, the specific capacitance value can be calculated using the following equation:[29]

$$C = \frac{I\Delta t}{m\Delta t} \quad (3)$$

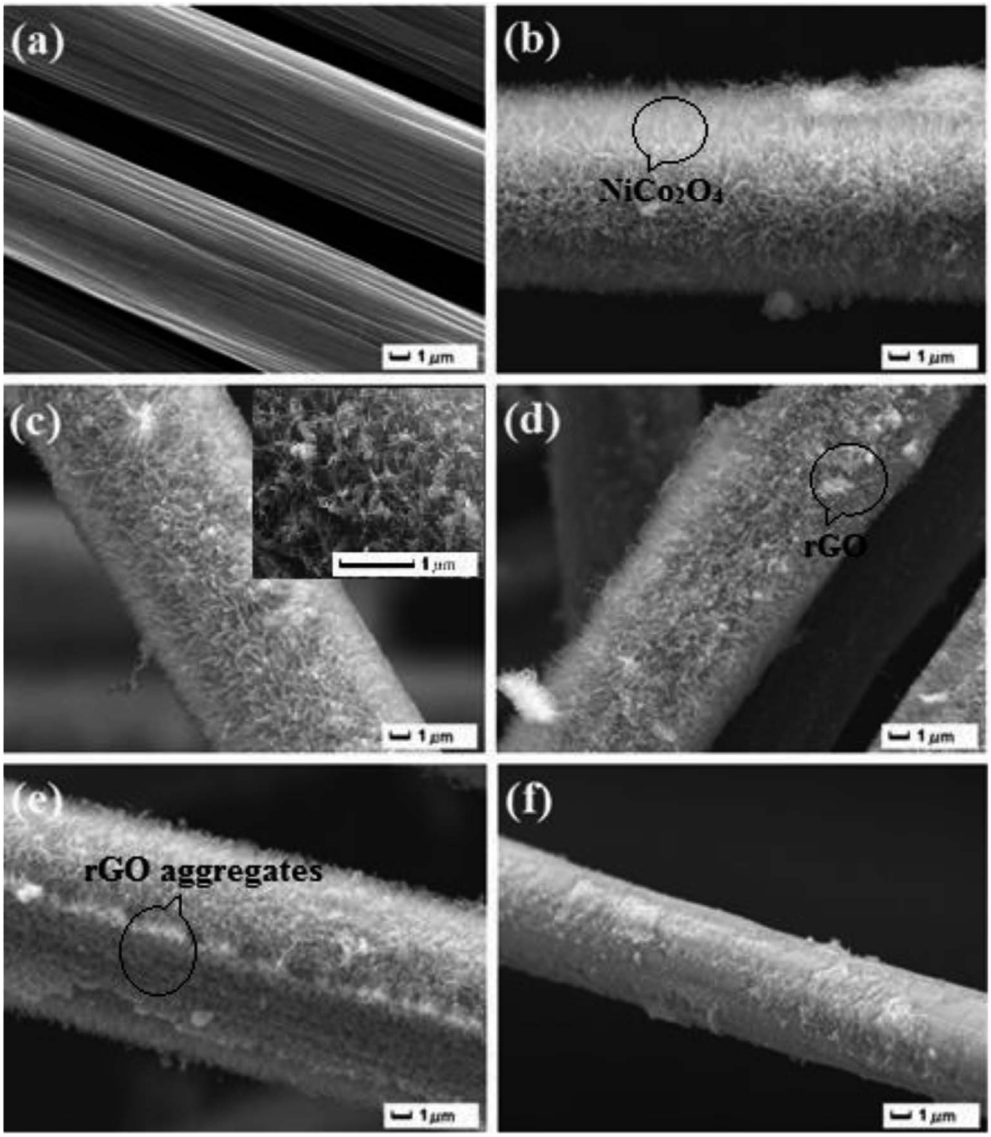

Fig. 2 SEM images of (a) CF and $NiCo_2O_4$/rGO/CF samples with different GO concentrations: (b) 0.2 mg ml^{-1}; (c) 0.4 mg ml^{-1}; (d) 0.6 mg ml^{-1}; (e) 0.8 mg ml^{-1} and (f) 1.0 mg ml^{-1}.

where C (F g^{-1}), m (g), ΔV (V), I (A) and Δt (s) stand for the specific capacitance, the mass of the active material, the potential window, the current and the time, respectively.

According to Fig. 4a and b, the CV and GCD curves of $NiCo_2O_4$/rGO/CF electrodes were apparently effected by the GO concentration. The specific capacitance of $NiCo_2O_4$/rGO/CF electrodes with different GO concentrations are presented in Fig. 4c. When the GO concentration was 0.4 mg ml^{-1}, benefiting from the hierarchical porous structure and the synergistic effects between reduced graphene oxides and $NiCo_2O_4$ nanowires, the maximum specific capacitance of 931.7 F g^{-1} was obtained, while that of $NiCo_2O_4$/CF electrode was 704.9 F g^{-1}. However, when the GO concentration reached 1.0 mg ml^{-1}, the specific capacitance of $NiCo_2O_4$/rGO/CF decreased to 707.2 F g^{-1}. As mentioned above, the hierarchical porous nanostructure is helpful for improving the electrochemical performance. Massive graphene aggregation could result in the collapse of $NiCo_2O_4$ nanowires, leading to the destruction of the hierarchical porous nanostructure and the decrease in the specific capacitance, which was in conformity with the SEM results.

To gain a better comparison of the capacitive behaviors of the samples, EIS was conducted in a frequency range of 0.1–100 kHz with an amplitude of 5 mV. Generally, the Nyquist plot contains two parts, one part is a semicircle arc in high-frequency region, in which the intercept at the real axis (Z') could reflect the solution resistance and the diameter of the semicircle could reflect the interfacial charge-transfer resistance (R_{ct}); the other part is a line in low-frequency region, and the slope of the straight line could reflect the electrolyte diffusion in electrode materials. According to Fig. 4d, there was no significant difference in the high frequency region while the intercept increased gradually and the slope of the straight line decreased with increasing GO concentration. The $NiCo_2O_4$/rGO/CF electrode with GO concentration of 0.4 mg ml^{-1} showed

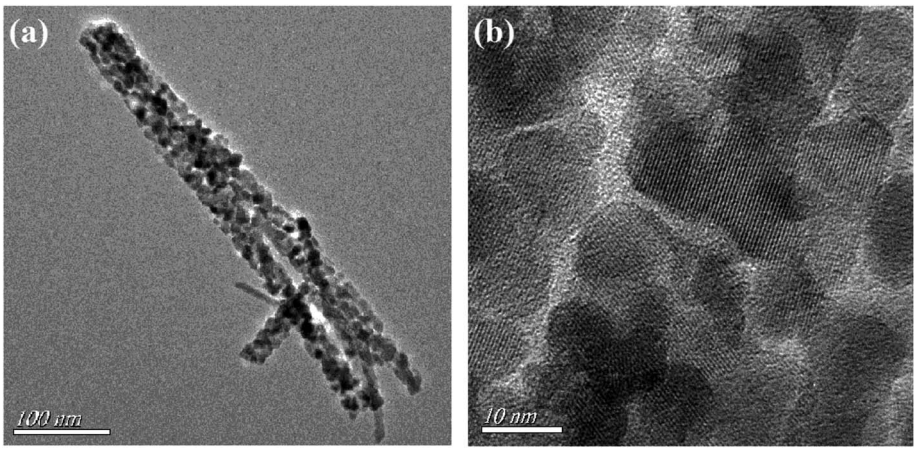

Fig. 3 (a) TEM and (b) HRTEM images of individual $NiCo_2O_4$ nanowire.

a steep slope shape in low-frequency region, indicating rapid ion diffusion in electrolyte and lower diffusion resistance,[30] which can be explained by the abundant pores and good conductive pathways between $NiCo_2O_4$ nanowires and rGO sheets. When the GO concentration increased, the slope of the straight lines decreased, indicating that the ion diffusion decreased, which might be due to the destruction of the hierarchical nanostructure caused by massive rGO aggregates. Results showed that GO concentration had remarkable effect on the structure and electrochemical performance of $NiCo_2O_4$/rGO/CF electrodes. It is important to construct the hierarchical porous nanostructure by controlling the GO content to obtain high-performance flexible supercapacitor electrodes.

3.3. Electrochemical performance of ACS device

To further assess the potential of $NiCo_2O_4$/rGO/CF electrodes in practical application, an asymmetric supercapacitor ($NiCo_2O_4$/

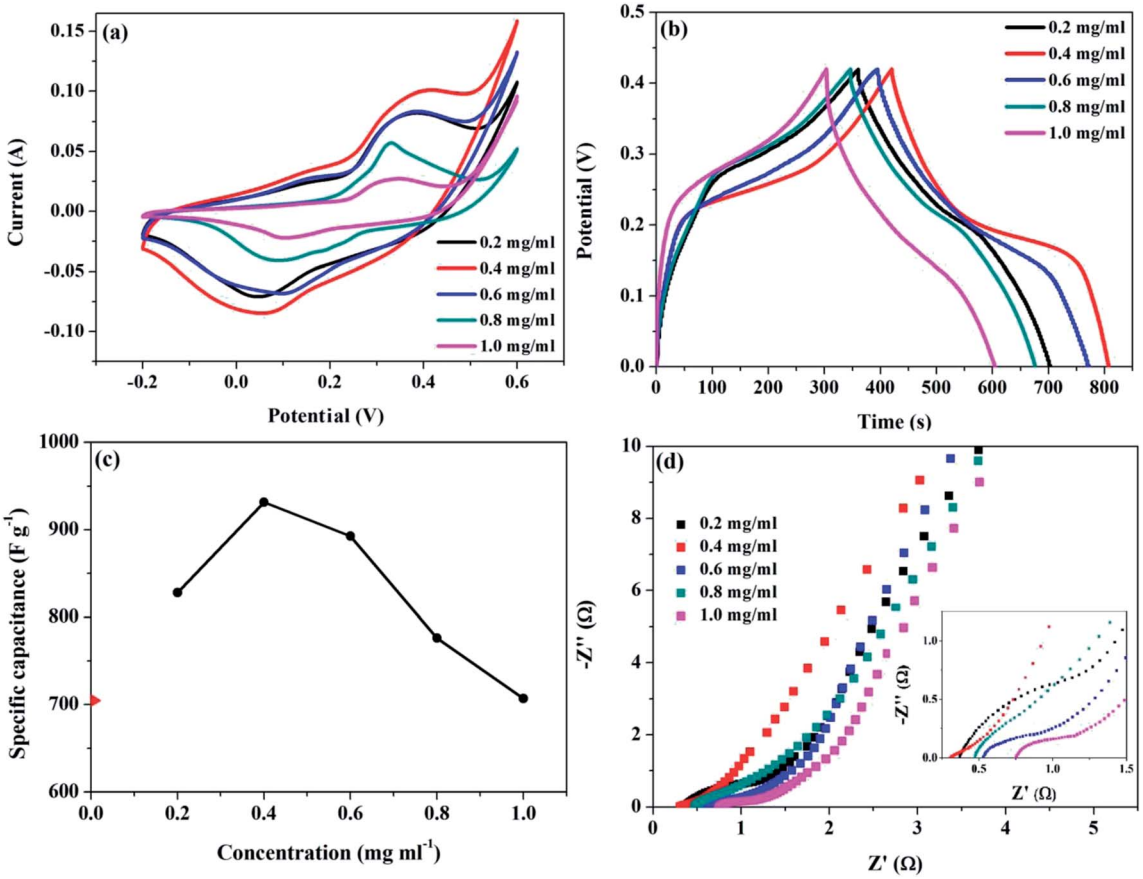

Fig. 4 (a) CV curves at 20 mV s^{-1}, (b) GCD curves at 1.0 A g^{-1}, (c) the specific capacitance and (d) EIS Nyquist spectra (the inset shows the enlarged plot) for $NiCo_2O_4$/rGO/CF electrodes.

rGO/CF//AC) was assembled, in which the $NiCo_2O_4$/rGO/CF and active carbon (AC) acted as the positive and negative electrodes, respectively.

The electrochemical properties of the $NiCo_2O_4$/rGO/CF//AC were illustrated in Fig. 5. The CV curves of the $NiCo_2O_4$/rGO/CF//AC supercapacitor within 0–1.7 V at different scan rates from 10 to 150 mV s^{-1} were depicted in Fig. 5a. As expected, the shapes of all CV curves maintained the same even at 150 mV s^{-1}, implying outstanding rate capability of the ASC device. From the GCD curves (Fig. 5b), it demonstrated that the capacitive behavior consisted of electric double layer and pseudo-capacitance characteristic. The specific capacitance values of the supercapacitor were illustrated in Fig. 5c. It showed that the maximum specific capacitance of 61.2 F g^{-1} at 1 A g^{-1} was achieved. When the current density was 10 A g^{-1}, the specific capacitance decreased to 41.8 F g^{-1}, and the capacitance

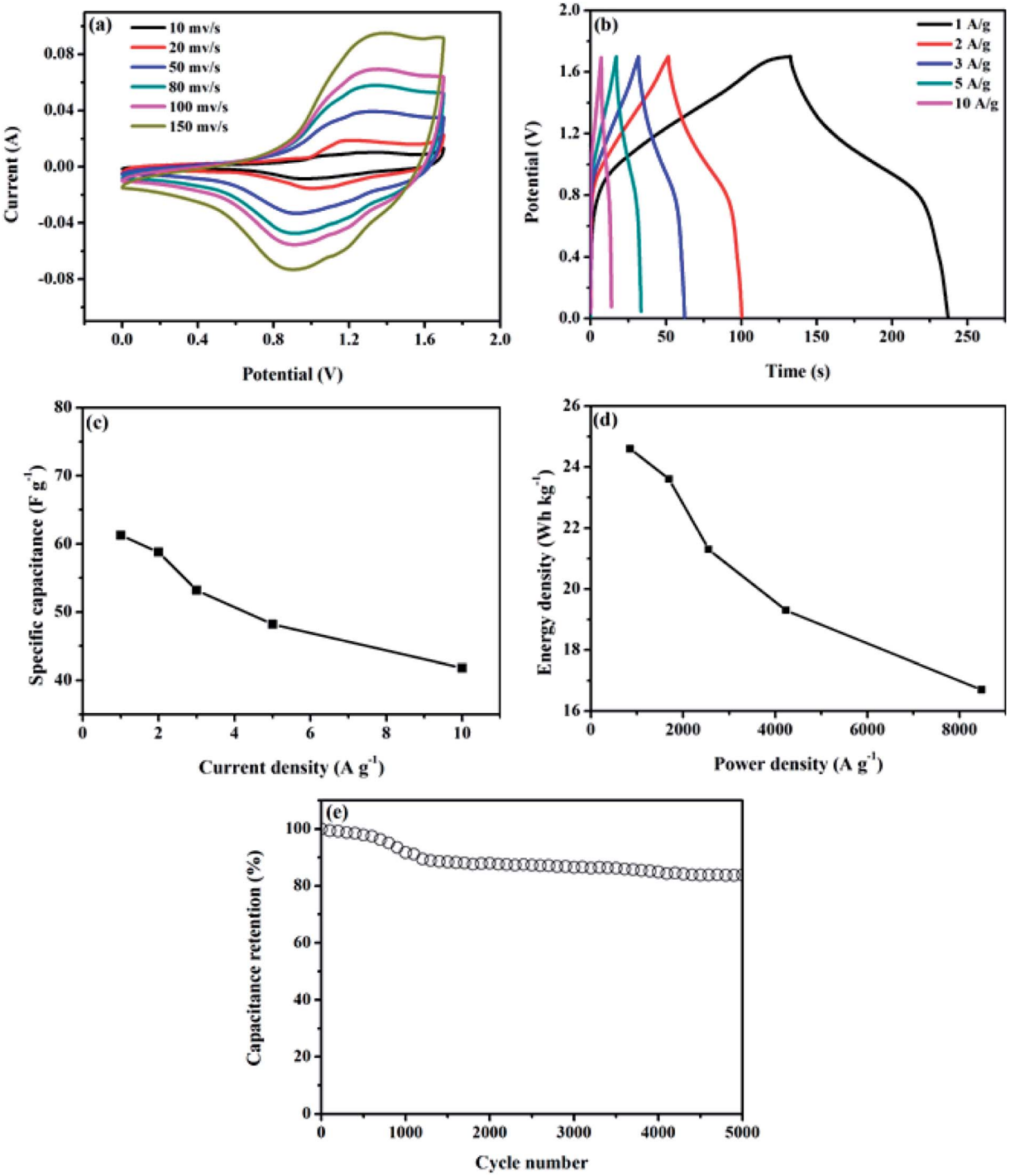

Fig. 5 Electrochemical properties of the $NiCo_2O_4$/rGO/CF//AC device: (a) CV curves at various scan rates, (b) GCD curves at different current densities, (c) the specific capacitance at various current densities, (d) Ragone plot and (e) cycling test.

retention was 68.3%. For supercapacitor, the energy density (E) and power density (P) are two main parameters, which can be calculated according to the following formulas:[31]

$$E = \frac{1}{7.2} CV^2 \quad (4)$$

$$P = \frac{E \times 3600}{\Delta t} \quad (5)$$

here C, V and Δt represent the specific capacitance of the device, the potential range, and the discharge time, respectively. The relationship between E and P can be described by the Ragone plot, as displayed in Fig. 5d. The as-obtained supercapacitor achieved a maximum energy density of 24.6 W h kg^{-1} with a power density of 850.3 W kg^{-1}, and a maximum power density of 8477.7 W kg^{-1} with an energy density of 16.7 W h kg^{-1}, which was superior to the reported MS/NCO//AC (18.4 W h kg^{-1} with a power density of 1200.2 W kg^{-1}),[32] $NiCo_2O_4$ NSs@HMRAs//AC (15.4 W h kg^{-1} with a power density of 700 W kg^{-1}),[33] and $FeSe_2$//$NiCo_2O_4$ (10.4 W h kg^{-1} with a power density of 0.2 kW kg^{-1})[34] devices. Moreover, the cycling life was evaluated by charge–discharge cycling at 2 A g^{-1}, as depicted in Fig. 5e, which exhibited 83.8% capacitance retention after 5000 cycles.

4. Conclusions

In summary, we have prepared the $NiCo_2O_4$/rGO/CF composites, in which rGO and $NiCo_2O_4$ nanowires were constructed on carbon fibers, forming hierarchical hybrid nanostructures. The effects of graphene oxide content on the structure and performance of the $NiCo_2O_4$/rGO/CF were in detail investigated. Results showed that the microstructure and electrochemical performance of the $NiCo_2O_4$/rGO/CF composites were affected significantly by GO content. As compared to $NiCo_2O_4$/CF with the specific capacitance of 704.9 F g^{-1}, benefiting from the hierarchical porous structure and the synergistic effects between reduced graphene oxide and $NiCo_2O_4$ nanowires, the $NiCo_2O_4$/rGO/CF composite with 0.4 mg ml^{-1} GO possessed a maximum specific capacitance of 931.7 F g^{-1} at 1 A g^{-1}. In addition, the $NiCo_2O_4$/rGO/CF//AC supercapacitor with a potential window of 1.7 V was assembled, which exhibited a maximum energy density of 24.6 W h kg^{-1} (at a power density of 850.3 W kg^{-1}) and a maximum power density of 8477.7 W kg^{-1} (at an energy density of 16.7 W h kg^{-1}), and delivered 83.8% capacitance retention over 5000 cycles. Results further demonstrated that the introduction of reduced graphene oxide could effectively improve the electrochemical performance of $NiCo_2O_4$/CF electrodes. However, the novel $NiCo_2O_4$/rGO/CF electrodes with controllable structure and excellent performance need to be further investigated to satisfy the needs of high-performance supercapacitors.

Conflicts of interest

There are no conflicts to declare.

Acknowledgements

This work was supported by Jiangsu University for Senior Intellectuals (No. 15JDG177).

References

1 H. Cheng, Z. Dong, C. Hu, Y. Zhao, Y. Hu, L. Qu, N. Chen and L. Dai, Highly nitrogen-doped carbon capsules: scalable preparation and high-performance applications in fuel cells and lithium ion batteries, *Nanoscale*, 2013, **5**, 2726–2733.

2 J. Zhi, W. Zhao, X. Liu, A. Chen, Z. Liu and F. Huang, Highly conductive ordered mesoporous carbon based electrodes decorated by 3D graphene and 1D silver nanowire for flexible supercapacitor, *Adv. Funct. Mater.*, 2014, **24**, 2013–2019.

3 L. Dong, C. Xu, Q. Yang, J. Fang, Y. Li and F. Kang, High-performance compressible supercapacitors based on functionally synergic multiscale carbon composite textiles, *J. Mater. Chem. A*, 2015, **3**, 4729–4737.

4 R. Wang, Y. Sui, S. Huang, Y. Pu and P. Cao, High-performance flexible all-solid-state asymmetric supercapacitors from nanostructured electrodes prepared by oxidation-assisted dealloying protocol, *Chem. Eng. J.*, 2018, **331**, 527–535.

5 P. H. Yang, Y. Ding, Z. W. Chen, Y. Z. Li, P. E. Qiang, M. Ebrahimi, W. J. Mai, C. P. Wong and Z. L. Wang, Low-cost high-performance solid-state asymmetric supercapacitors based on MnO_2 nanowires and Fe_2O_3 nanotubes, *Nano Lett.*, 2014, **14**, 731–736.

6 B. Liu, J. Zhang, X. F. Wang, G. Chen, D. Chen, C. W. Zhou and G. Z. Shen, Hierarchical three-dimensional $ZnCo_2O_4$ nanowire arrays/carbon cloth anodes for a novel class of high-performance flexible lithium-ion batteries, *Nano Lett.*, 2012, **12**, 3005–3011.

7 Y. K. Hsu, Y. C. Chen, Y. G. Lin, L. C. Chen and K. H. Chen, High-cell-voltage supercapacitor of carbon nanotube/carbon cloth operating in neutral aqueous solution, *J. Mater. Chem.*, 2012, **22**, 3383–3387.

8 W. Ren, C. Wang, L. F. Lu, D. D. Li, C. W. Cheng and J. P. Liu, SnO_2@Si core-shell nanowire arrays on carbon cloth as a flexible anode for Li ion batteries, *J. Mater. Chem. A*, 2013, **1**, 13433–13438.

9 Q. Q. Xiong, J. P. Tu, X. H. Xia, X. Y. Zhao, C. D. Gu and X. L. Wang, A three-dimensional hierarchical Fe_2O_3@NiO core/shell nanorod array on carbon cloth: a new class of anode for high-performance lithium-ion batteries, *Nanoscale*, 2013, **5**, 7906–7912.

10 W. L. Yang, Z. Gao, J. Ma, X. M. Zhang, J. Wang and J. Y. Liu, Hierarchical $NiCo_2O_4$@NiO core-shell hetero-structured nanowire arrays on carbon cloth for a high-performance flexible all-solid-state electrochemical capacitor, *J. Mater. Chem. A*, 2014, **2**, 1448–1457.

11 R. B. Rakhi, W. Chen, D. Cha and H. Alshareef, Substrate dependent self-organization of mesoporous cobalt oxide

nanowires with remarkable pseudocapacitance, *Nano Lett.*, 2012, **12**, 2559–2567.

12 L. Shen, Q. Che, H. Li and X. Zhang, Mesoporous $NiCo_2O_4$ nanowire arrays grown on carbon textiles as binder-free flexible electrodes for energy storage, *Adv. Funct. Mater.*, 2014, **24**, 2630–2637.

13 X. Lu, M. Yu, G. Wang, T. Zhai, S. Xie, Y. Ling, Y. Tong and Y. Li, H-TiO_2@MnO_2//H-TiO_2@C core– shell nanowires for high performance and flexible asymmetric supercapacitors, *Adv. Mater.*, 2013, **25**, 267–272.

14 L. Hu, W. Chen, X. Xie, N. Liu, Y. Yang, H. Wu, Y. Yao, M. Pasta, H. N. Alshareef and Y. Cui, Symmetrical MnO_2-carbon nanotube-textile nanostructures for wearable pseudocapacitors with high mass loading, *ACS Nano*, 2011, **5**, 8904–8913.

15 J. Xu, Q. Wang, X. Wang, Q. Xiang, B. Liang, D. Chen and G. Z. Shen, Flexible asymmetric supercapacitors based upon Co_9S_8 nanorod//Co_3O_4@RuO_2 nanosheet arrays on carbon cloth, *ACS Nano*, 2013, **7**, 5453–5462.

16 X. Lu, G. Wang, T. Zhai, M. Yu, S. Xie, Y. Ling, C. Liang, Y. Tong and Y. Li, Stabilized TiN nanowire arrays for high-performance and flexible supercapacitors, *Nano Lett.*, 2012, **12**, 5376–5381.

17 R. Tamilselvi, N. Padmanathan, K. Mani Rahulan, P. Mohana Priya, R. Sasikumar and M. Mandhakini, Reduced graphene oxide (rGO): supported NiO, Co_3O_4 and $NiCo_2O_4$ hybrid composite on carbon cloth (CC)–bi-functional electrode/catalyst for energy storage and conversion devices, *J. Mater. Sci.: Mater. Electron.*, 2018, **29**, 4869–4880.

18 N. Padmanathan, S. Selladurai and K. Razeeb, Ultra-fast rate capability of a symmetric supercapacitor with a hierarchical Co_3O_4 nanowire/nanoflower hybrid structure in non-aqueous electrolyte, *RSC Adv.*, 2015, **5**, 12700–12709.

19 N. Padmanathan and S. Selladurai, Controlled growth of spinel NiCoO nanostructures on carbon cloth as a superior electrode for supercapacitors, *RSC Adv.*, 2014, **4**, 8341–8349.

20 N. Padmanathan, S. Han, S. Selladurai, C. Glynn, C. O'Dwyer and K. M. Razeeb, Pseudocapacitance of α-$CoMoO_4$ nanoflakes in non-aqueous electrolyte and its bi-functional electro catalytic activity for methanol oxidation, *Int. J. Hydrogen Energy*, 2015, **40**, 16297–16305.

21 Q. F. Wang, X. F. Wang, B. Liu, G. Yu, X. J. Hou, D. Chen and G. Z. Shen, $NiCo_2O_4$ nanowire arrays supported on Ni foam for high-performance flexible all-solid-state supercapacitors, *J. Mater. Chem. A*, 2013, **1**, 2468–2473.

22 G. Q. Zhang, H. B. Wu, H. E. Hoster, M. B. Chan-Park and X. W. Lou, Single-crystalline $NiCo_2O_4$ nanoneedle arrays grown on conductive substrates as binder-free electrodes for high-performance supercapacitors, *Energy Environ. Sci.*, 2012, **5**, 9453–9456.

23 D. Kong, W. Ren, C. Cheng, Y. Wang, Z. Huang and H. Yang, Three-dimensional $NiCo_2O_4$@polypyrrole coaxial nanowire arrays on carbon textiles for high-performance flexible asymmetric solid-state supercapacitor, *ACS Appl. Mater. Interfaces*, 2015, **7**, 21334–21346.

24 T. Chen, Y. Fan, G. Wang, J. Zhang, H. Chuo and R. Yang, Rationally designed carbon Fiber@$NiCo_2O_4$@polypyrrole core–shell nanowire array for high-performance supercapacitor Electrodes, *Nano*, 2016, **11**, 1650–1655.

25 C. Nethravathi and M. Rajamathi, Chemically modified graphene sheets produced by the solvothermal reduction of colloidal dispersions of graphite oxide, *Carbon*, 2008, **46**, 1994–1999.

26 L. Pan, H. Zhao, W. Shen, X. Dong and J. Xu, Surfactant-assisted synthesis of a Co_3O_4/reduced graphene oxide composite as a superior anode material for Li-ion batteries, *J. Mater. Chem. A*, 2013, **1**, 7159–7166.

27 J. Qi, Y. Chang, Y. Sui, Y. He, Q. Meng, F. Wei, Y. Ren and Y. Jin, Facile Synthesis of Ag-Decorated Ni_3S_2 Nanosheets with 3D Bush Structure Grown on rGO and Its Application as Positive Electrode Material in Asymmetric Supercapacitor, *Adv. Mater. Interfaces*, 2018, **5**, 1700985.

28 T. Wang, Y. Guo, B. Zhao, S. Yu, H. P. Yang, Da. Lu, X. Z. Fu, R. Sun and C. P. Wong, $NiCo_2O_4$ nanosheets *in situ* grown on three dimensional porous Ni film current collectors as integrated electrodes for high-performance supercapacitors, *J. Power Sources*, 2015, **286**, 371–379.

29 Q. Tang, M. Chen, L. Wang and G. Wang, A novel asymmetric supercapacitors based on binder-free carbon fiber paper@nickel cobaltite nanowires and graphene foam electrodes, *J. Power Sources*, 2015, **273**, 654–662.

30 X. Liu, F. Wei, Y. Sui, J. Qi, Y. He and Q. Meng, Polyhedral ternary oxide $FeCo_2O_4$: A new electrode material for supercapacitors, *J. Alloys Compd.*, 2018, **735**, 1339–1343.

31 Y. Ding, W. Bai, J. Sun, Y. Wu, M. A. Memon, C. Wang, C. Liu, Y. Huang and J. Geng, Cellulose Tailored Anatase TiO_2 Nanospindles in Three-Dimensional Graphene Composites for High-Performance Supercapacitors, *ACS Appl. Mater. Interfaces*, 2016, **8**, 12165–12175.

32 S. Wen, Y. Liu, F. Zhu, R. Shao and W. Xua, Hierarchical MoS_2 nanowires/$NiCo_2O_4$ nanosheets supported on Ni foam for high-performance asymmetric supercapacitors, *Appl. Surf. Sci.*, 2018, **428**, 616–622.

33 X. F. Lu, D. J. Wu, R. Z. Li, Q. Li, S. H. Ye, Y. X. Tong and G. R. Li, Hierarchical $NiCo_2O_4$ Nanosheets@Hollow Microrod Arrays for High-performance Asymmetric Supercapacitors, *J. Mater. Chem. A*, 2014, **2**, 4706–4713.

34 C. Ji, F. Liu, L. Xu and S. Yang, Urchin-like $NiCo_2O_4$ hollow microspheres and $FeSe_2$ micro-snowflakes for flexible solid-state asymmetric supercapacitors, *J. Mater. Chem. A*, 2017, **5**, 5568–5576.